Annihilations of Antiprotons at Rest in Hydrogen. IV. $\bar{p}p \to \bar{K}K\pi\pi$†

N. BARASH, L. KIRSCH, D. MILLER,* AND T. H. TAN§
Columbia University, New York, New York
(Received 23 December 1965)

In a study of 735 000 antiproton annihilations at rest in the hydrogen bubble chamber, 3424 events of the reaction $\bar{p}+p \to K\bar{K}\pi\pi$ were observed. We present here the invariant-mass distributions and scatterplots for this reaction, separated according to the three channels $K_1K_1\pi^+\pi^-$, $K_1(K^0)\pi^+\pi^-$, and $K_1K^\pm\pi^\mp\pi^0$. Also presented are branching ratios into the various channels. K^* production is found to dominate in all cases. The fraction of $\bar{p}p$ annihilations into $K^*\bar{K}^*$ is $(4.5\pm0.9)\times10^{-3}$, and into $K^*K\pi$ is $(7.7\pm1.7)\times10^{-3}$.

I. INTRODUCTION

As a continuation of our study of antiproton annihilations at rest, we present here the results of the experimental study of the reactions

$$\bar{p}+p \to K^0\bar{K}^0\pi^+\pi^-$$
$$\bar{p}+p \to K^0K^\pm\pi^\mp\pi^0.$$

We shall present and discuss the scattergrams, invariant-mass distributions, and annihilation rates for the various charge channels. The results have been, in part, reported earlier.[1] Some of the results of a similar study by Armenteros *et al.*[2] have been published.

II. EXPERIMENTAL TECHNIQUE

This study is based on an exposure of the Columbia-BNL 30-in. hydrogen bubble chamber to a low-energy separated beam at the Brookhaven AGS. Approximately 630 000 pictures, containing 735 000 stopped antiprotons were analyzed.

The scanners were instructed to select all events consisting of an antiproton annihilation into two charged prongs plus one or two V's. The events having these topologies were measured and processed using the Nevis Laboratories spatial-reconstruction program NP54.[3] The GRIND kinematics program[4] was used to fit the V's to the three-constraint hypothesis $K_1^0 \to \pi^+\pi^-$.

At the antiproton-annihilation vertex, events with two V's were fitted to the four-constraint hypothesis:

$$\bar{p}p \to K_1^0K_1^0\pi^+\pi^- \quad 491 \text{ events.} \quad (1)$$

Events with one V were fitted to the one-constraint hypotheses:

$$\bar{p}p \to K_1^0(K^0)\pi^+\pi^- \quad 1418 \text{ events,} \quad (2)$$
$$\to K_1^0K^\pm\pi^\mp(\pi^0) \quad 1910 \text{ events.} \quad (3)$$

where the particles enclosed in parentheses are unseen. An event was accepted if the $\chi^2 \leq 5\times$(number of constraints). For the one-V events an additional requirement was that the apparent track density, as estimated by the measurer, be consistent with the calculated ionization for the hypothesis. The number of accepted events is given in (1)–(3).

Of the one-V events 339 are acceptable as both $K_1^0(K^0)\pi^+\pi^-$ and $K_1^0K^\pm\pi^\mp(\pi^0)$. These ambiguous events are plotted in all distributions to which they may belong, although in the determination of annihilation rates a corrected number of events has been used. The correction also accounts for losses due to true $K^\pm K^0\pi^\mp(\pi^0)$ or $K_1^0(K^0)\pi^+\pi^-$ events, which failed either in the fitting process or in the ionization test.

The corrected numbers of events were determined by using the accepted two-V events to simulate the one-V events. These pseudo one-V events were subject to the same acceptance criteria as the observed events. From the fraction of these events which fit $K_1^0(K^0)\pi^+\pi^-$ alone, we estimate the true number of events in reaction

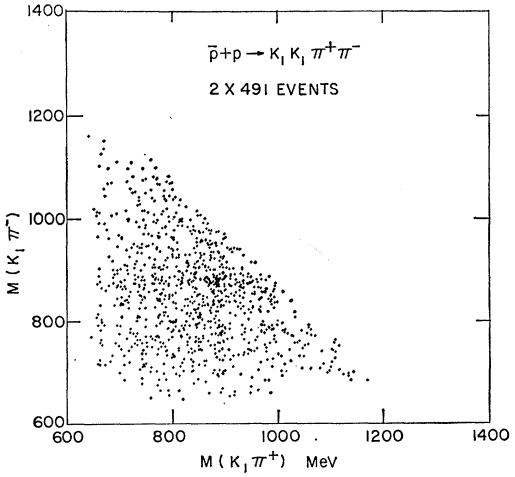

FIG. 1. Triangle plot of $m(K_1\pi^+)$ versus $m(K_1\pi^-)$ for the reaction $\bar{p}+p \to K_1K_1\pi^+\pi^-$.

† Work supported in part by the U. S. Atomic Energy Commission.
* Present address: Massachusetts Institute of Technology, Cambridge, Massachusetts.
§ Present address: Stanford Linear Accelerator Center, Stanford University, Stanford, California.
[1] N. Barash, P. Franzini, L. Kirsch, D. Miller, J. Steinberger, and T. H. Tan, in *Proceedings of the 12th Annual International Conference on High-Energy Physics, Dubna, 1964* (Atomizdat, Moscow, 1965).
[2] R. Armenteros, D. N. Edwards, T. Jacobsen, L. Montanet, J. Vandermeulen, C. d'Andlau, A. Astier, P. Baillon, J. Cohen-Ganouna, C. Defoix, J. Siaud, and P. Rivet, in *Proceedings of the 12th Annual International Conference on High-Energy Physics, Dubna, 1964* (Atomizdat, Moscow, 1965); R. Armenteros, D. N. Edwards, T. Jacobsen, L. Montanet, A. Shapira, J. Vandermeulen, C. d'Andlau, A. Astier, P. Baillon, J. Cohen-Ganouna, C. Defoix, J. Siaud, C. Ghesquiere, and P. Rivet, Phys. Letters **9**, 207 (1964).
[3] R. J. Plano, D. H. Tycko, Nucl. Instr. Methods **20**, 458 (1963).
[4] R. Böck, CERN Report No. 61-29, 1961 (unpublished).

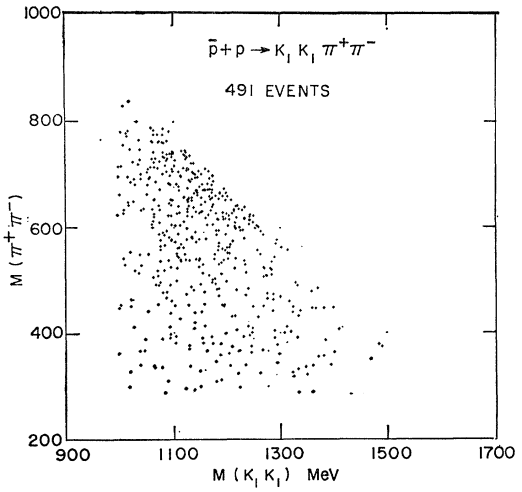

FIG. 2. Triangle plot of $m(K_1K_1)$ versus $m(\pi^+\pi^-)$ for the reaction $\bar{p}+p \rightarrow K_1K_1\pi^+\pi^-$.

(2) to be 1550±90. The true number of events in reaction (3) is estimated to be 1790±100 events. The branching ratios into a given channel will be calculated, using these corrected numbers, and not the observed numbers.

III. RESULTS

The results of this experiment are displayed in the scattergrams of Figs. 1–7 and in the KK, $\pi\pi$, $K\pi$, $K\pi\pi$, and $KK\pi$ combined mass plots of Figs. 8–13. The smooth curve drawn on the histograms represents the invariant phase space for the reaction $\bar{p}+p \rightarrow K\bar{K}\pi\pi$, normalized to the total numbers of events.

A. Final-State Production Rates

In order to obtain the branching ratios for annihilation into the various channels, it is necessary to know

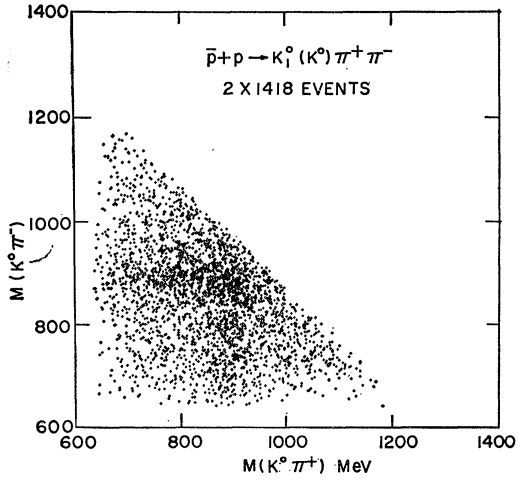

FIG. 3. Triangle plot of $m(K^0\pi^+)$ versus $m(K^0\pi^-)$ for the reaction $\bar{p}+p \rightarrow K_1(K^0)\pi^+\pi^-$.

the $\bar{p}$ flux and the efficiencies for observing and retaining events:

1. Flux. From a count of antiprotons in 18 000 frames distributed over 50% of the film, we estimate the total number of antiprotons in the entire exposure to be $(7.35\pm0.74)\times10^5$. After correcting for annihilation in flight, this corresponds to $(6.32\pm.74\times)10^5$ antiprotons which annihilate at rest.

2. Scanning Efficiency. All film was scanned twice. From the rescan and selected triple scannings, we estimate a scanning efficiency of 0.95±0.05.

3. Geometrical Detection Efficiency. There is a loss of K_1^0's due to the finite size of the chamber, and the difficulty of observing events which decay close to the annihilation vertex. These losses are approximated by an efficiency function which is unity between 0.2 and 12.0 cm and zero elsewhere. Using the average K^0

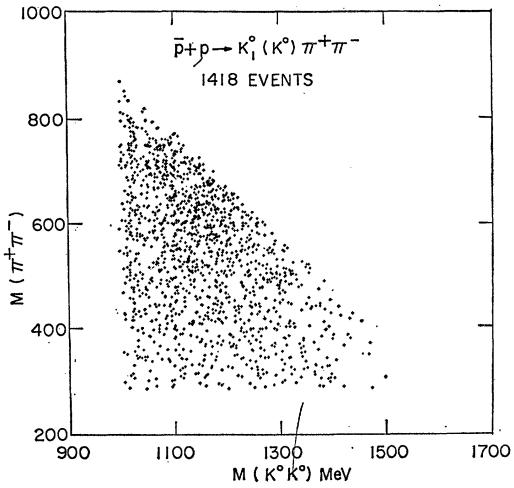

FIG. 4. Triangle plot of $m(K^0K^0)$ versus $m(\pi^+\pi^-)$ for the reaction $\bar{p}+p \rightarrow K_1(K^0)\pi^+\pi^-$.

momentum of 350 MeV/c, the detection efficiency for observing $K_1^0 \rightarrow \pi^+\pi^-$ is 0.91±0.03.

4. Reconstruction Efficiency. The events which failed in the spatial reconstruction program were not remeasured. The corresponding efficiency of an event surviving reconstruction is 0.86±0.04 for reaction (1) and 0.91±0.03 for reactions (2) and (3).

5. K_1^0 Decay. The charged decay branching ratio of the K_1^0 is given by[5]

$$(K_1^0 \rightarrow \pi^+\pi^-)/(K_1^0 \rightarrow \text{all}) = 0.7\pm0.05.$$

From the corrected number of events fitting reactions (1)–(3), we can determine the total rate of antiproton annihilations into channels $K_1^0K_1^0\pi^+\pi^-$, $K_1^0K_2^0\pi^+\pi^-$, and $K_1^0K^\pm\pi^\mp\pi^0$. In order to obtain the branching ratios,

[5] A. Rosenfeld *et al.*, Rev. Mod. Phys. **36**, 977 (1964).

we first define the following efficiencies:

α is the probability of observing $K_1^0K_1^0\pi^+\pi^-$ as a two-V event.

$$\alpha = (\text{reconstruction efficiency}) \times (\text{probability of charged } K_1^0 \text{ decay})^2 \times (\text{geometric detection efficiency})^2 = 0.349, \quad (4)$$

β is the probability of observing $K_1^0K_1^0\pi^+\pi^-$ as a one-V event.

$$\beta = 2\times(\text{reconstruction efficiency}) \times (\text{probability of charged } K_1^0 \text{ decay}) \times (\text{geometric detection efficiency}) \times [(\text{probability of neutral } K_1^0 \text{ decay}) + (\text{probability of unobserved charged } K_1^0 \text{ decay})] = 0.416, \quad (5)$$

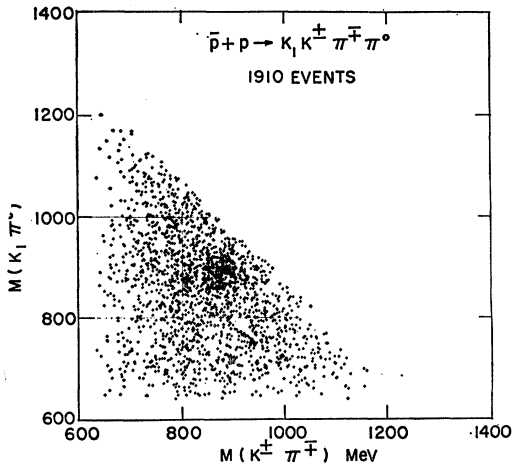

FIG. 5. Triangle plot of $m(K^{\pm}\pi^{\mp})$ versus $m(K_1\pi^0)$ for the reaction $\bar{p}+p \to K_1K^{\pm}\pi^{\mp}\pi^0$.

γ is the probability of observing $K_1^0K_2^0\pi^+\pi^-$ or $K_1^0K^{\pm}\pi^{\mp}\pi^0$ as a one-V event.

$$\gamma = (\text{reconstruction efficiency}) \times (\text{probability of charged } K_1^0 \text{ decay}) \times (\text{geometric detection efficiency}) = 0.574. \quad (6)$$

The total number of $K_1^0K_1^0\pi^{\mp}\pi^0$ events is given by

$$[\text{Number fitting reaction (1)}]/\alpha.$$

The number of $K_1^0K_2^0\pi^+\pi^-$ events is determined by subtracting the number of $K_1^0K_1^0\pi^+\pi^-$, which would be observed in the reaction $K_1^0(K^0)\pi^+\pi^-$, from the total number in this reaction, and is given by $(1/\gamma)$ {number fitting reaction $(2)-(\beta/\alpha)\times$[number fitting reaction (1)]}.

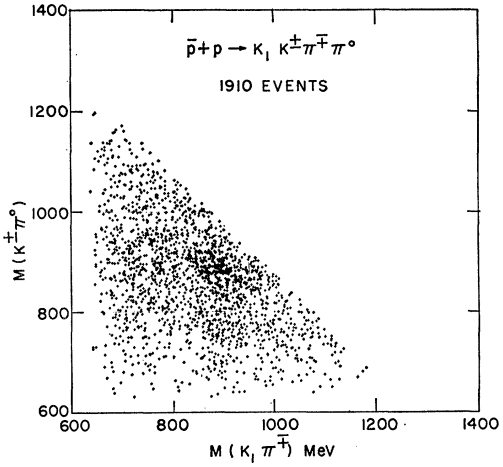

FIG. 6. Triangle plot of $m(K_1\pi^{\mp})$ versus $m(K^{\pm}\pi^0)$ for the reaction $\bar{p}+p \to K_1K^{\pm}\pi^{\mp}\pi^0$.

The total number of $K_1^0K^{\pm}\pi^{\mp}\pi^0$ events is given by

$$[\text{Number fitting reaction (3)}]/\gamma.$$

Thus, using the $\bar{p}$ flux and scanning efficiency, we obtain the rates:

$$\bar{p}p \to K_1^0K_1^0\pi^+\pi^- \quad (2.33\pm0.30)\times10^{-3},$$
$$\bar{p}p \to K_1^0K_2^0\pi^+\pi^- \quad (2.79\pm0.42)\times10^{-3},$$
$$\bar{p}p \to K^{\pm}K_1^0\pi^{\mp}\pi^0 \quad (5.19\pm0.61)\times10^{-3}.$$

B. K^* Production Rates

The four-body final-state $K\bar{K}\pi\pi$ can proceed through the intermediate states

$$\bar{p}p \to K^*K\pi$$
$$\to K^*\bar{K}^*.$$

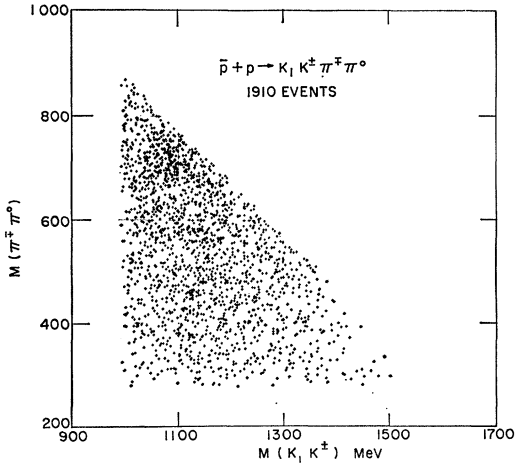

FIG. 7. Triangle plot of $m(K_1K^{\pm})$ versus $m(\pi^{\mp}\pi^0)$ for the reaction $\bar{p}+p \to K_1K^{\pm}\pi^{\mp}\pi^0$.

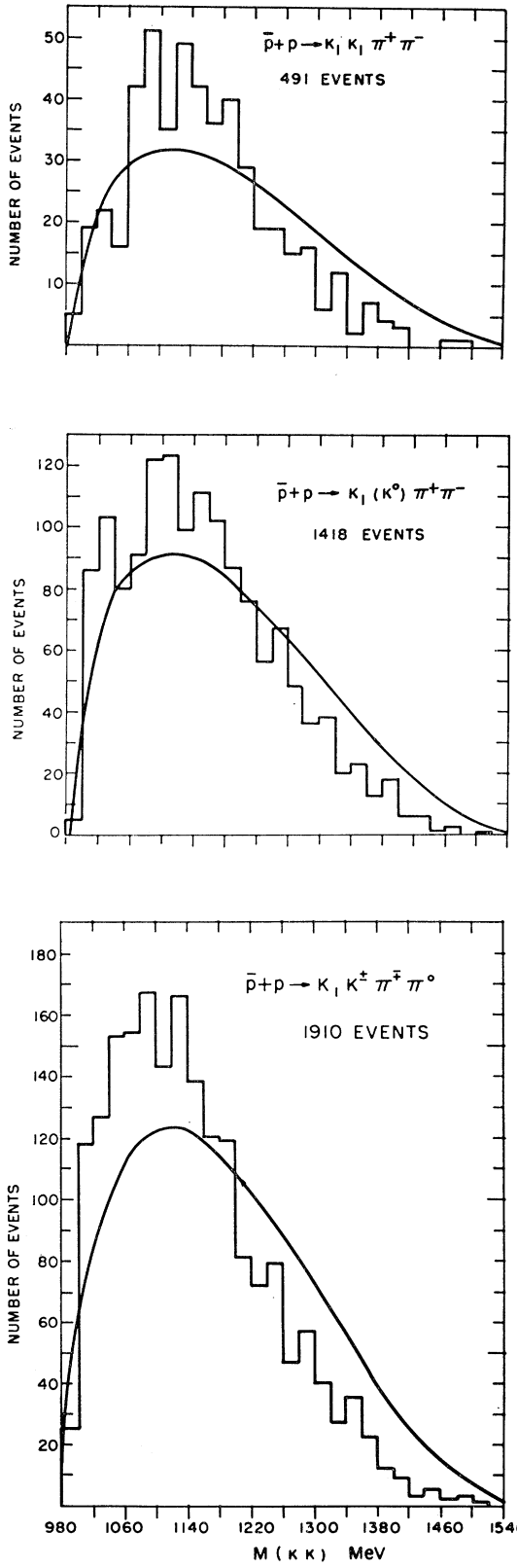

FIG. 8. Histogram of the (KK) invariant mass for the reactions $\bar{p}+p \to K_1 K_1 \pi^+\pi^-$, $\bar{p}+p \to K_1(K^0)\pi^+\pi^-$, $\bar{p}+p \to K_1 K^\pm \pi^\mp \pi^0$.

It is apparent from the scattergrams of Figs. 1–7 that both states are present, although in amounts that vary in the different charge channels. In order to estimate the rates for these processes we have fitted the scattergrams in the region of $K\pi$ combined mass indicated in Fig. 14. The theoretical function used to describe the data assumes a constant matrix element plus Breit-Wigner resonance functions. We also assume no interference between the various amplitudes contributing to the process.

Let us define BW_+, BW_-, BW_0, $BW_{\bar{0}}$, to be Breit-Wigner resonance distributions in the K^{*+}, K^{*-}, K^{*0}, and $\bar{K}^{*0}$ mass, respectively, and ϕ to be the invariant phase space function of the dynamical variances.

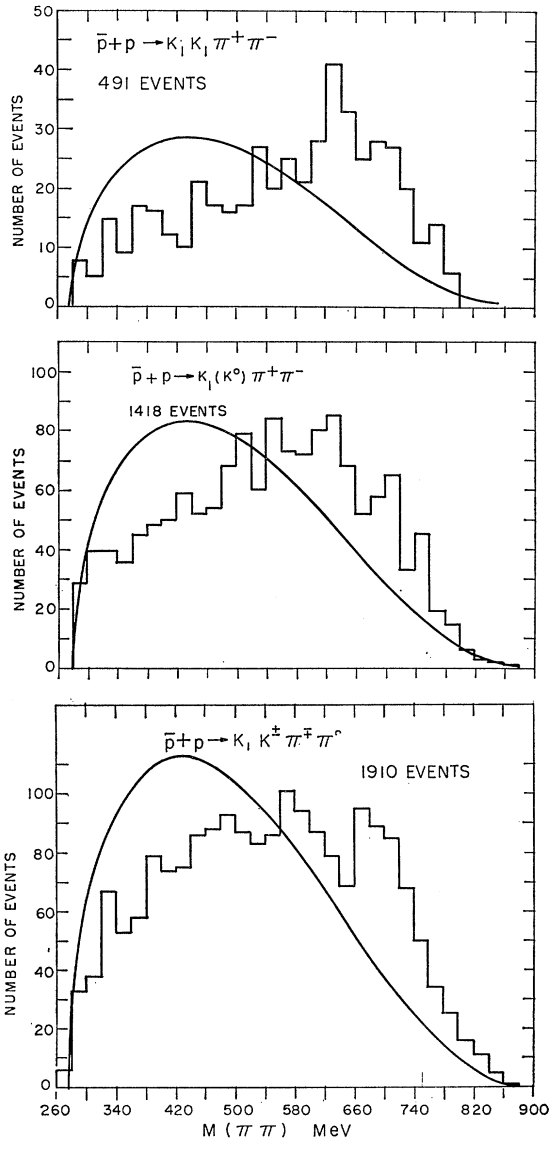

FIG. 9. Histogram of the $(\pi\pi)$ invariant mass for the reactions $\bar{p}+p \to K_1 K_1 \pi^+\pi^-$, $\bar{p}+p \to K_1(K^0)\pi^+\pi^-$, $\bar{p}+p \to K_1 K^\pm \pi^\mp \pi^0$.

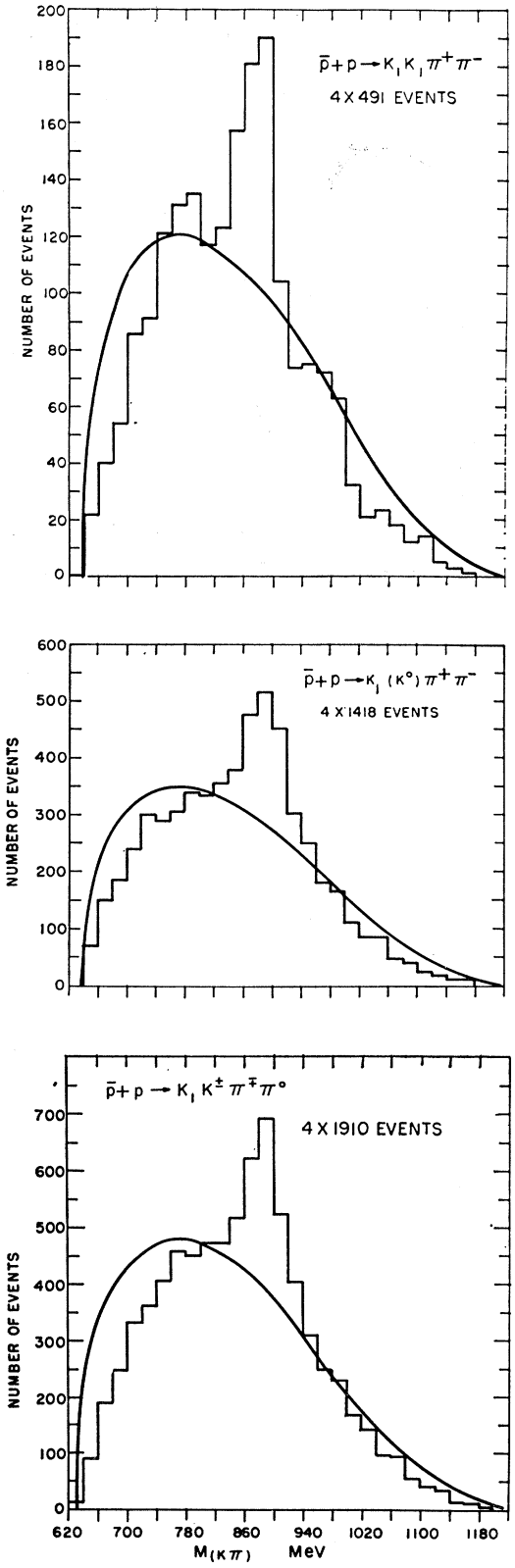

FIG. 10. Histogram of the $(K\pi)$ invariant mass for the reactions $\bar{p}+p \to K_1\bar{K}_1\pi^+\pi^-$, $\bar{p}+p \to K_1(K^0)\pi^+\pi^-$, $\bar{p}+p \to K_1K^\pm\pi^\mp\pi^0$.

$$\mathrm{BW}=(\tfrac{1}{2}\Gamma)/[(m_{K\pi}-m_{K^*})^2+(\tfrac{1}{2}\Gamma)^2],$$
$$m_{K^*}=890 \text{ MeV},$$
$$\Gamma=50 \text{ MeV}.$$

For reactions (1) and (2) the transition rate is taken to be of the form

$$(a_1+a_2\mathrm{BW}_+ +a_3\mathrm{BW}_- +a_4\mathrm{BW}_+\times\mathrm{BW}_-)\phi. \quad (7)$$

Here, a_1 is the nonresonant intensity, a_2 and a_3 measure the contributions of single K^{*+} and K^{*-} production, respectively, and a_4 is the contribution of double K^* production.

For reaction (3) the transition rate is

$$(b_1+b_2\mathrm{BW}_+ +b_3\mathrm{BW}_- +b_4\mathrm{BW}_+ \times\mathrm{BW}_- +b_5\mathrm{BW}_0+b_6\mathrm{BW}_{\bar{0}}+b_7\mathrm{BW}_0\times\mathrm{BW}_{\bar{0}})\phi. \quad (8)$$

The a_i and b_i are taken as free parameters in the fit.

The branching ratios for double-K^* production were determined by first dividing the scatterplots in the region indicated in Fig. 14, into 15 bins, each 60×60-

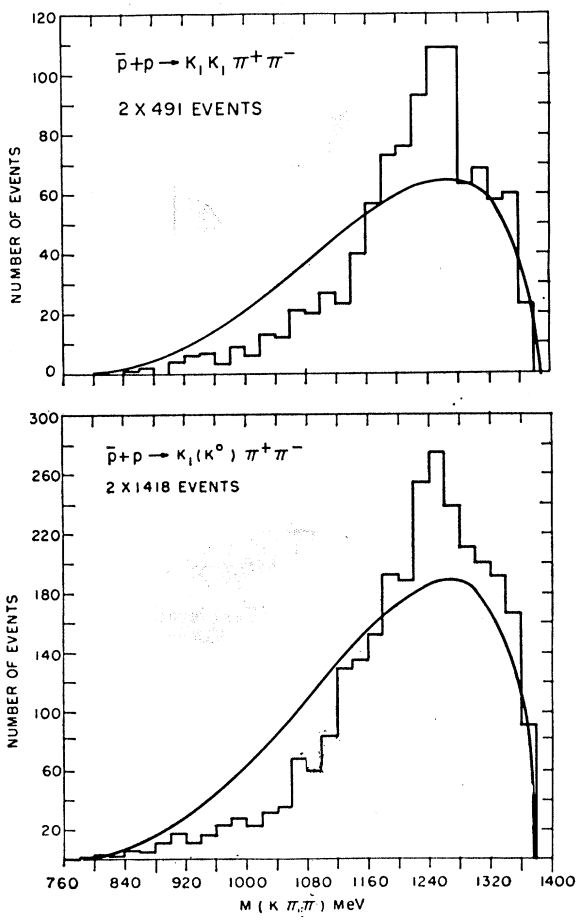

FIG. 11. Histogram of the $(K\pi\pi)$ invariant mass for the reactions $\bar{p}+p \to K_1K_1\pi^+\pi^-$, $\bar{p}+p \to K_1(K^0)\pi^+\pi^-$.

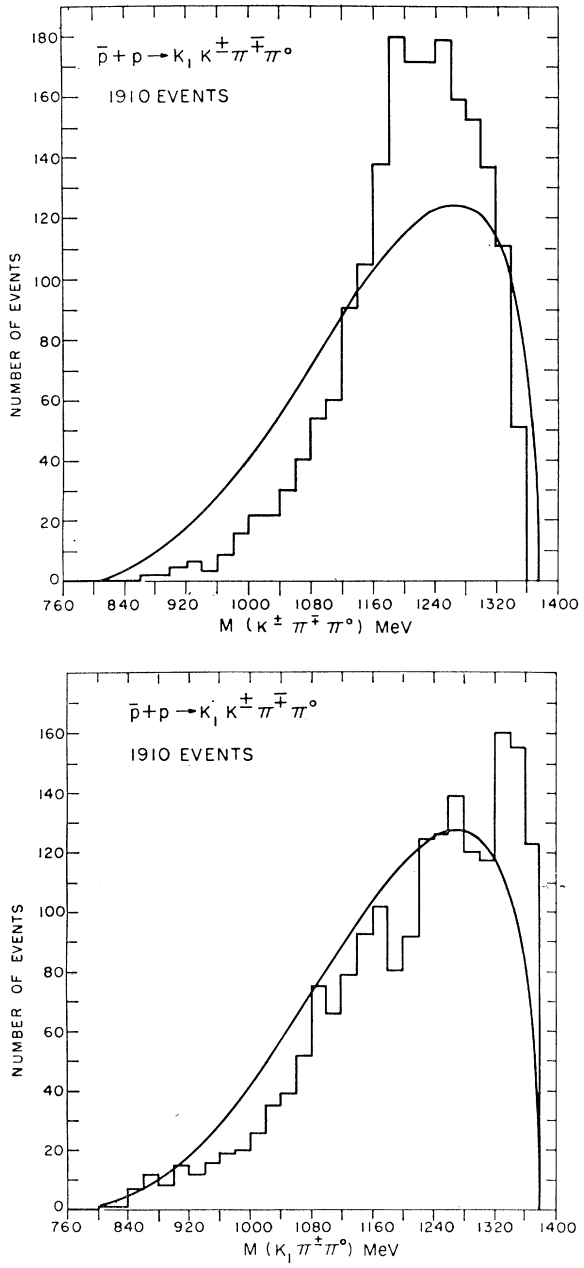

FIG. 12. Histogram of the $(K\pi\pi)$ invariant mass for the reaction $\bar{p}+p \to K_1 K^{\pm}\pi^{\mp}\pi^0$.

MeV wide. A Monte Carlo program was used to generate $KK\pi\pi$ events according to the distributions (7) and (8). In the case of reactions (1) and (2), each Monte Carlo event was plotted twice on the same graph for each of the two possible $K\pi$ associations. A least-squares fit was made by comparing the number of Monte Carlo events in a bin for each term of (7) and (8) to the number of observed events in the same bin.

The total number of K^*'s produced in each channel was determined by fitting the $K\pi$ histograms in the region 720–1040 MeV, assuming the background can be described by a function which is a quadratic in the $K\pi$ mass. The results are given in Table I.

We note that for reaction (1), the K^* rate observed here is $(59\pm11)\%$, which is not in agreement with the result of Armenteros *et al.*, who observe no appreciable K^* production in this channel. The results contained in Table I can be used to determine the absolute rates for

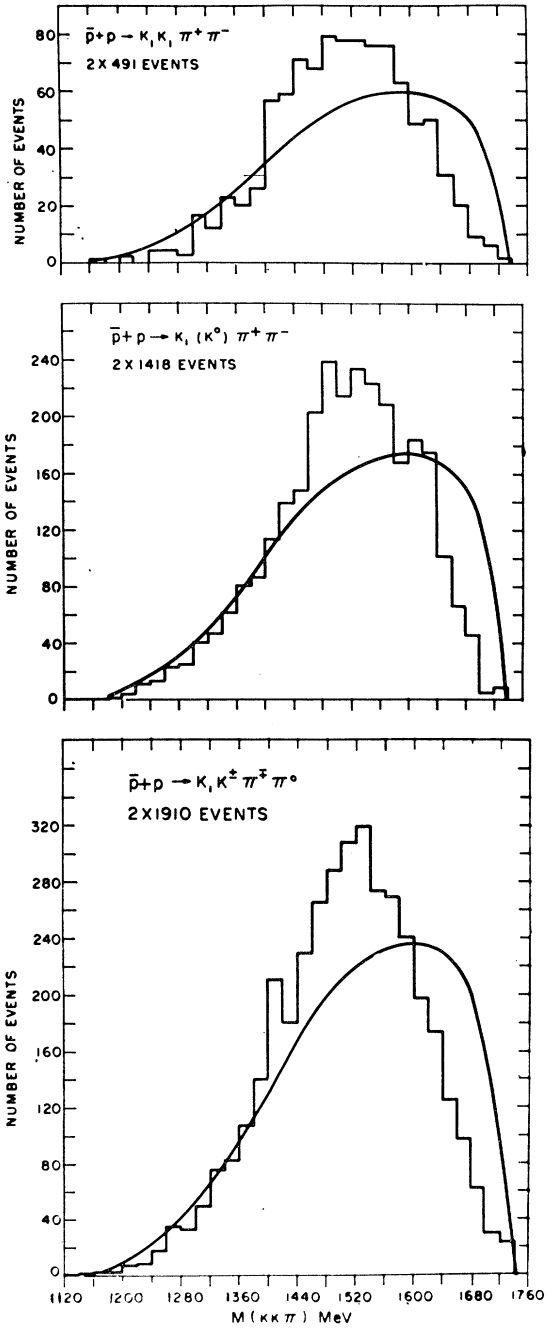

FIG. 13. Histogram of the $(KK\pi)$ invariant mass for the reactions $\bar{p}+p \to K_1 K_1 \pi^+\pi^-$, $K_1(K^0)\pi^+\pi^-$, $\bar{p}+p \to K_1 K^{\pm}\pi^{\mp}\pi^0$.

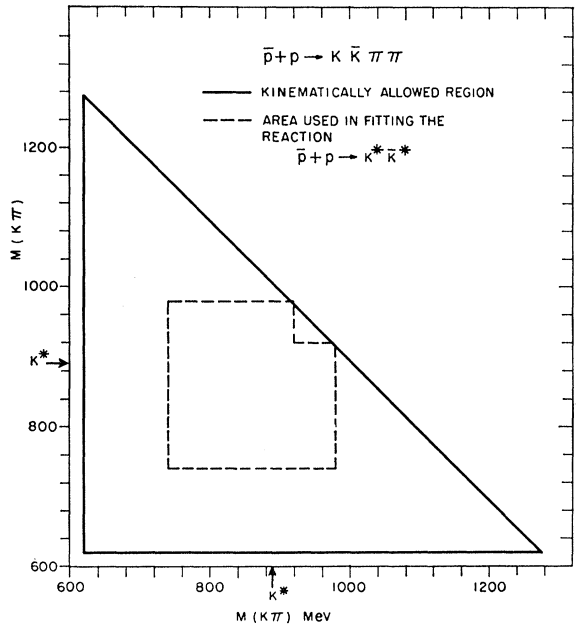

FIG. 14. The kinematically allowed region for a plot of $m(K_a\pi_a)$ versus $m(K_b\pi_b)$ for the reaction $\bar{p}+p \to K_aK_b\pi_a\pi_b$. The area outlined by the dashed line indicates that region which was used in fitting for the reaction $\bar{p}+p \to K^*\bar{K}^*$.

annihilations which proceed via K^* production into the final states $K^0\bar{K}^0\pi^+\pi^-$ and $K^0K^\pm\pi^\mp\pi^0$. The final state $K^0\bar{K}^0\pi^+\pi^-$ is related to the observed rates for K_1^0 and K_2^0 production by

$$\Gamma(K^0\bar{K}^0\pi^+\pi^-)=2\Gamma(K_1^0K_1^0\pi^+\pi^-)+\Gamma(K_1^0K_2^0\pi^+\pi^-).$$

The rate for $K_1^0K_2^0\pi^+\pi^-$ is obtained in the same manner as in Sec. A by subtraction of $K_1^0K_1^0\pi^+\pi^-$ events from $K_1^0(K^0)\pi^+\pi^-$. From the values given in Table I and the antiproton flux, we obtain the annihilation rates given in Table II.

TABLE I. Number of K^* events produced in $\bar{p}p \to K\bar{K}\pi\pi$.

Reaction	Number of events
(1) $\bar{p}+p \to K_1K_1\pi^+\pi^-$	Total number of events = 491±22
	Total number of K^*'s = 289±51
$\to K^{*\pm}K^0\pi^\mp$	137±101
$\to K^{*+}K^{*-}$	76±44
(2) $\bar{p}+p \to K_1(K^0)\pi^+\pi^-$	Total number of events = 1550±90
	Total number of K^*'s = 1047±95
$\to K^{*\pm}K^0\pi^\mp$	971±208
$\to K^{*+}K^{*-}$	38±93
(3) $\bar{p}+p \to K_1^0K^\pm\pi^\mp\pi^0$	Total number of events = 1790±100
	Total number of $K^{*\pm}$ = 621±66
	Total number of K^{*0} = 514±65
$\to K^{*0}K^\pm\pi^\mp$	98±64
$\to K^{*0}K_1^0\pi^0$	~ 0
$\to K^{*\pm}K_1^0\pi^\mp$	180±77
$\to K^{*\pm}K^\mp\pi^0$	168±75
$\to K^{*+}K^{*-}$	138±59
$\to K^{*0}\bar{K}^{*0}$	246±44

TABLE II. Fraction of antiproton annihilations producing K^*'s.

Final state of $K^0\bar{K}^0\pi^+\pi^-$	Rate
$\bar{p}+p \to K^{*\pm}K^0\pi^\mp$	$(3.63\pm0.97)\times10^{-3}$
$\to K^{*+}K^{*-}$	$(0.57\pm0.37)\times10^{-3}$
Final state $K^0K^\pm\pi^\mp\pi^0$	Rate
$\bar{p}+p \to K^{*0}K^\pm\pi^\mp$	$(0.57\pm0.38)\times10^{-3}$
$\to K^{*\pm}K^\mp\pi^0$	$(0.97\pm0.45)\times10^{-3}$
$\to K^{*\pm}K^0\pi^\mp$	$(1.04\pm0.45)\times10^{-3}$
$\to K^{*+}K^{*-}$	$(0.77\pm0.32)\times10^{-3}$
$\to K^{*0}\bar{K}^{*0}$	$(1.43\pm0.30)\times10^{-3}$

We note that isotopic-spin invariance predicts the following relationships between the rates for K^* production:

$$\frac{K^{*+}K^{*-} \to K^0\bar{K}^0\pi^+\pi^-}{K^{*+}K^{*-} \to K^0K^\pm\pi^\mp\pi^0}=1$$

and

$$\frac{K^{*\pm}K^0\pi^\mp \to K^0\bar{K}^0\pi^+\pi^-}{K^{*\pm}K^0\pi^\mp \to K^0K^\pm\pi^\mp\pi^0}=2.$$

Experimentally, we obtain for these ratios 0.74±0.58 and 3.48±1.77, in agreement with the predicted values.

The observed channels represent only a fraction of the total annihilation rate into K^*'s. Using isospin invariance, we obtain the total K^* rates, which are given in Table III.

C. Other Resonances

1. ρ and ϕ. The four-body final state can proceed through the intermediate states:

$$\bar{p}p \to K\bar{K}\rho$$
$$\to \phi\pi^+\pi^-.$$

As can be seen from Fig. 9, the phase-space curve for the $\pi\pi$ combined mass differs everywhere substantially from the data. Thus, it would be unreasonable to attempt to estimate the amount of ρ production by fitting the data to the assumption of a constant matrix element plus a Breit-Wigner curve for the ρ.

The ϕ would be observed near the lower kinematic limit of the KK combined-mass distribution. In this region the phase space is changing rapidly, making it difficult to estimate the amount of ϕ production.

TABLE III. Total branching ratios for antiproton annihilation into K^*'s.

Reaction	Branching ratio
$\bar{p}+p \to K^{*+}K^{*-}$	$(1.5\pm0.6)\times10^{-3}$
$\bar{p}+p \to K^{*0}\bar{K}^{*0}$	$(3.0\pm0.7)\times10^{-3}$
$\bar{p}+p \to K^{*\pm}K^{0}\pi^{\mp}$	$(4.6\pm1.0)\times10^{-3}$
$\bar{p}+p \to K^{*\pm}K^{\mp}\pi^{0}$	$(1.4\pm0.7)\times10^{-3}$
$\bar{p}+p \to K^{*0}K^{\pm}\pi^{\mp}$	$(1.7\pm1.2)\times10^{-3}$
$\bar{p}+p \to K^{*0}K^{0}\pi^{0}$	~0

Based upon observations of the ϕ in the reaction $\bar{p}p \to K^+K^-\pi^+\pi^-$, we would expect seventy-five ϕ events in $K_1^0(K^0)\pi^+\pi^-$.[6] Our data are compatible with this number.

2. C^0. Armenteros *et al.*[2] have analyzed the $K\pi\pi$ and $\pi\pi$ mass plots by assuming the existence of a $(K\pi\pi)^0$ resonance of mass 1215 MeV and a width of 60 MeV. These authors observe the C^0 to decay into $K^0\rho^0$ 80% of the time. They observe no enhancement in the $(K\pi\pi)^\pm$ combination at the same mass.

We observe similar deviations from phase space in the neutral $K\pi\pi$ mass distribution. To test the C^0 hypothesis, we have attempted simultaneously to fit the five invariant mass distributions KK, $\pi\pi$, $K\pi$, $K\pi\pi$, and $KK\pi$ from reactions (1) and (2). In addition to pure phase space we have assumed that the following intermediate states may be present:

$$\bar{p}p \to C^0K^0 \searrow \begin{cases} K^0\pi^+\pi^- \\ K^0\rho^0 \\ K^{*\pm}\pi^{\mp} \end{cases} \to K^{*\pm}K^0\pi^{\mp}.$$

The method of least squares was used to determine the relative amount of each state. We failed to obtain what seemed to us a reasonable fit to the five distributions. Because of this, we do not know whether this deviation from phase space constitutes a resonance, or is due to some other property of the antiproton-annihilation matrix elements.

[6] D. Miller, Nevis Report No. 131 (unpublished).

ACKNOWLEDGMENTS

We would like to thank Professor J. Steinberger and Professor P. Franzini for many helpful suggestions and discussions in the course of this work. We would also like to thank Professor R. J. Plano and the Rutgers Bubble Chamber Group for help in the early stages of the experiment. We are grateful to the operating crews of the 30-in. hydrogen bubble chamber and the AGS staff at Brookhaven National Laboratory for their help in the exposure. Finally, we thank the scanning and measuring staffs of the Rutgers and Nevis laboratories for their excellent work.